A Simulation Model for SiC MOSFET Switching Transients Controlled by an Adaptive Gate Driver with the Capability of Reducing Switching Losses and EMI across the Full Operating Range

[1]Zheming Li, [2]Robert W. Maier, [1]Mark-M. Bakran, [3]Franz-J. Niedernostheide, [3]Daniel Domes

[1]University of Bayreuth, Center of Energy Technology, Department of Mechatronics
[1]Universitätsstraße 30
[1]Bayreuth, Germany

[2]ZF Friedrichshafen AG
[2]Am Briefzentrum 2
[2]Bayreuth, Germany

[3]Infineon Technologies AG
[3]Am Campeon 1-15
[3]Neubiberg, Germany

Tel.: +49 / (0) – 921 55 7811
E-Mail: zheming.li@uni-bayreuth.de
URL: https://www.mechatronik.uni-bayreuth.de

Keywords

«Intelligent gate driver», «Device simulation», «EMC/EMI», «Switching losses», «Silicon Carbide (SiC)», «MOSFET».

Abstract

In this paper, the performance of an intelligent-gate-driver-based self-regulating gate control approach, which can reduce switching losses and EMI at SiC MOSFET turn-off and turn-on, is investigated by simulation and verified by measurements. Firstly, a MOSFET behavior model is presented and confirmed with double pulse measurement results of this approach. Based on this model, the performance of this approach in continuous operation is evaluated and compared with measurement in continuous operation. It is verified that there is a good match between measurement and simulation. The trade-off between switching losses and EMI is improved significantly by the proposed gate control approach compared to simple gate control with a single gate resistance.

1 Introduction

In recent years, wide bandgap semiconductors like SiC MOSFETs are in the process of replacing Si IGBTs in many power electronic applications. SiC MOSFETs show many advantages, such as low conduction and switching losses. But there are some challenges. Generally, fast switching transients are desired for low switching losses. However, the switching speed of SiC MOSFETs is limited by the drain-source overvoltage and the voltage oscillation, which are both induced by the commutation circuit stray inductance and the latter causes electromagnetic interference (EMI) emission [1-2]. Besides, the usually unwanted parasitic turn-on (PTO) effect [3-4], which occurs during the turn-on switching transients of a SiC MOSFET in a half-bridge configuration and results in a temporary shoot-through current of the phase, tends to increase at higher switching speed.

Active gate drivers (AGDs) are utilized to ensure a better compromise between switching losses and EMI emission of SiC MOSFET switching transients. A comprehensive overview of the state-of-the-art SiC devices AGD research is provided in [5]. The control strategies of AGD are classified into 3 categories, as shown in column 2-4 of Table I. The open-loop control shown in column 2 of Table I applies the same driver voltage profile to all scenarios. Yet optimum switching performance cannot be guaranteed in most operating conditions, as power electronic applications normally have a wide operating range. The direct feedback control shown in column 3 of Table I uses sensor circuits to detect the feedback signals. Their references are tracked by adapting the output of AGD. However, adjusting the gate control parameters of AGD during switching transients needs high speed, high-bandwidth electrical components like sensors, A/D converters, comparators, which are not economy friendly. Besides, even with these expensive components, their propagation delay and the parasitic effects of the AGD circuit

may lead to insufficient switching performance. The model-based indirect control shown in column 4 of Table I estimates the feedback indices with an accurate switching trajectory model of power devices instead of direct measurement or describes the relation between operating parameters and gate control parameters with a look-up-table. Operating parameters like DC-link voltage, load current and junction temperature are sensed prior to each switching process to derive the optimum gate control parameters with the model or the look-up-table. No ultrafast components are required to detect the high frequent feedback signals. However, new problems such as high computation load of AGD, enormous calibration and measuring efforts are introduced. Moreover, measuring inaccuracies may lead to insufficient results.

Table I: Comparison between AGD control strategies in [5] and the proposed approach

AGD control strategies	Open-loop control [5]	Direct feedback control [5]	Model-based indirect control [5]	**Proposed approach**
Description	Applying constant gate control parameters for all operating conditions	Compensating errors between measured feedback signals and references via adjusting control parameters during actual switching transient	Building look-up-table/switching trajectory model to derive switching performance and gate control parameters	**Adjusting control parameters for the next switching event according to EMI evaluation of the actual one**
Feedback signals	No	$\mathrm{d}u/\mathrm{d}t$, $\mathrm{d}i/\mathrm{d}t$, $u_{DS}(t)$, $i_D(t)$, T_j etc.	U_{DC}, I_D, T_j etc.	**$\mathrm{d}i/\mathrm{d}t$ for EMI evaluation**
Operating condition dependence	Not considered	Considered	Considered	**Considered**
Requirements on driver-hardware	Low	High speed, high-bandwidth sensors, comparators, processors etc. with low propagation delay	Measurement of relevant operating parameters, high computation load of AGD, etc.	**Measurement and processing of $\mathrm{d}i/\mathrm{d}t$-signal with low timing requirements**
Calibration effort	Low	Low	High	**Low**
Cost	Low	High	High	**Low**
Performance in operation	--	**(--, ++)** depending on switching speed	+	**Evaluated in this work**

An AGD-based self-regulating gate control approach is proposed in [6-7] and shown in column 5 of Table I. It consists of two methods, a boost-method for the optimization of a single operating point and a tracking method for the closed-loop control of varying operating conditions. The boost-method provides two levels of switching speed. Both levels are used successively in one switching process. It is verified in [6-7] by double pulse measurements that the boost-method can realize low switching losses and low switching oscillation at a certain operating point at both of SiC MOSFET turn-off and turn-on, when the gate control parameters are set as optimum. The control loop of the tracking method is closed not in the actual switching event, but over the next one. The drain-current slope $\mathrm{d}i/\mathrm{d}t$ is measured by the voltage drop from the power source to the kelvin source of SiC devices for oscillation evaluation by a simple comparator. The gate control parameters are adjusted for the next switching process according to the oscillation evaluation of the actual switching process. The adjustment is conducted after the actual and before the next switching process. Thanks to sufficient time between two successive switching events, the timing requirements for the $\mathrm{d}i/\mathrm{d}t$-signal-processing are low. Furthermore, measurement of operating parameters or establishment of an accurate model or look-up-table is unnecessary. Therefore, hardware, calibration and measuring efforts are reduced significantly.

In this paper, a SiC MOSFET switching trajectory model is presented. The accuracy of this model is confirmed by double pulse measurements of the proposed gate control approach. Simulations of PWM controlled continuous operation are performed with this approach and compared with measurements performed under the same test condition. The performance of this approach is evaluated and compared to the performance of simple gate control with a single gate resistance.

2 Measurement setup and SiC MOSFET behavior simulation model

The devices under test (DUTs) are 1.7 kV SiC MOSFETs in TO-247 package. The rated current of a single chip is 37.5 A. The double pulse experiment is used to investigate the switching behavior of the SiC MOSFETs. All the experiments are performed as single chip measurements, where the commutation circuit stray inductance (L_σ) is scaled to emulate the switching behavior of a high power module, as shown in [8].

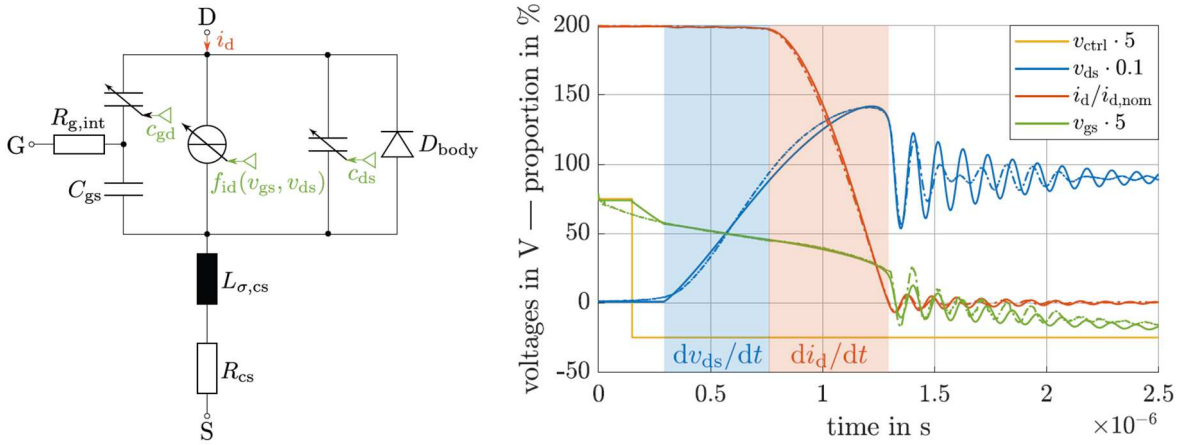

(a) Schematic of the SiC MOSFET simulation model

b) Comparison between measurement (dash-dotted) and simulation (solid) in a high inductive setup

Fig. 1: Schematic and results of the SiC MOSFET simulation model [9-10]

The SiC MOSFET behavior simulation model is shown in Fig. 1 (a). This model is proposed and explained in detail in [9-10]. With this model, the switching processes can be described with a small number of input parameters. The voltage-dependent MOSFET capacitances c_{ds}, c_{gd} and the constant capacitance C_{gs} can be received from capacity measurements or data sheet. The measurement of the common source elements $L_{\sigma,\,cs}$ and R_{cs} is explained in [9]. The central function of the model i_d (v_{gs}, v_{ds}) can be acquired by measurements of transfer characteristics. Finally, the switching environment including the scaled commutation circuit stray inductance and gate resistances is needed. A comparison between a double pulse measurement shown in dash-dotted lines and the corresponding simulation shown in solid lines is shown in Fig. 1 (b). The accuracy of the model is verified.

3 Optimization of switching performance for a single operating point

In this section, the variant of the boost-method shown in [6] for the optimization of SiC MOSFET turn-off switching performance and the variant shown in [7] for the optimization of turn-on switching performance are briefly reviewed, respectively. The simulated and the measured switching trajectories are compared to verify the accuracy of the proposed simulation model.

3.1 Optimization of turn-off switching performance

The working principle of the boost-method implemented at SiC MOSFET turn-off is shown in Fig. 2 (a). The low boost gate resistance $R_{G,\,boost\text{-}off}$ accelerates the switching speed, whereas the high gate resistance $R_{G,\,normal}$ suppresses the drain-source voltage oscillation. The control signal (green), the output voltages of the normal-driver $U_{DR,\,normal}$ (blue) and the boost-driver $U_{DR,\,boost}$ (red) at SiC MOSFET turn-off are shown in Fig. 2 (a) right. When a turn-off switching process is initiated, $U_{DR,\,normal}$ switches from the positive driver voltage U_P to the negative U_N and maintains U_N until the next turn-on switching process. $U_{DR,\,boost}$ is normally U_P. It changes to U_N at the start of the turn-off switching process for a predefined time duration called boost-time t_B. The diode D_{off} ensures that $R_{G,\,boost\text{-}off}$ is only active and accelerates the switching speed during boost-time. A comparison between three switching processes performed without (dashed with high switching speed, dotted with low switching speed) and with the boost-method (solid) is shown in Fig. 2 (b). With the boost-method low switching losses and low oscillation are achieved simultaneously.

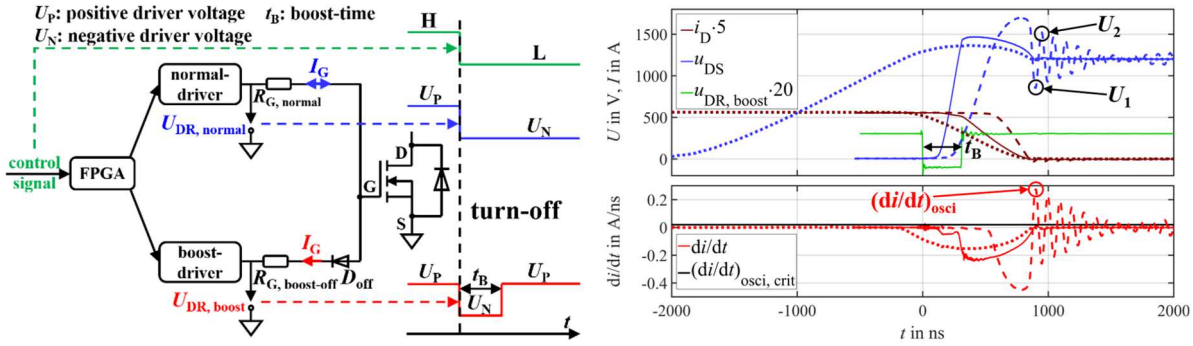

(a) Working principle of the boost-method implemented at SiC MOSFET turn-off with the control signal and output voltages of gate drivers

(b) Comparison between switching events with (solid) and without (dashed, dotted) the boost-method at U_{DC} = 1.2 kV, I_D = 112 A, T_j = 25°C

Fig. 2: A brief review of the boost-method implemented at SiC MOSFET turn-off [6]

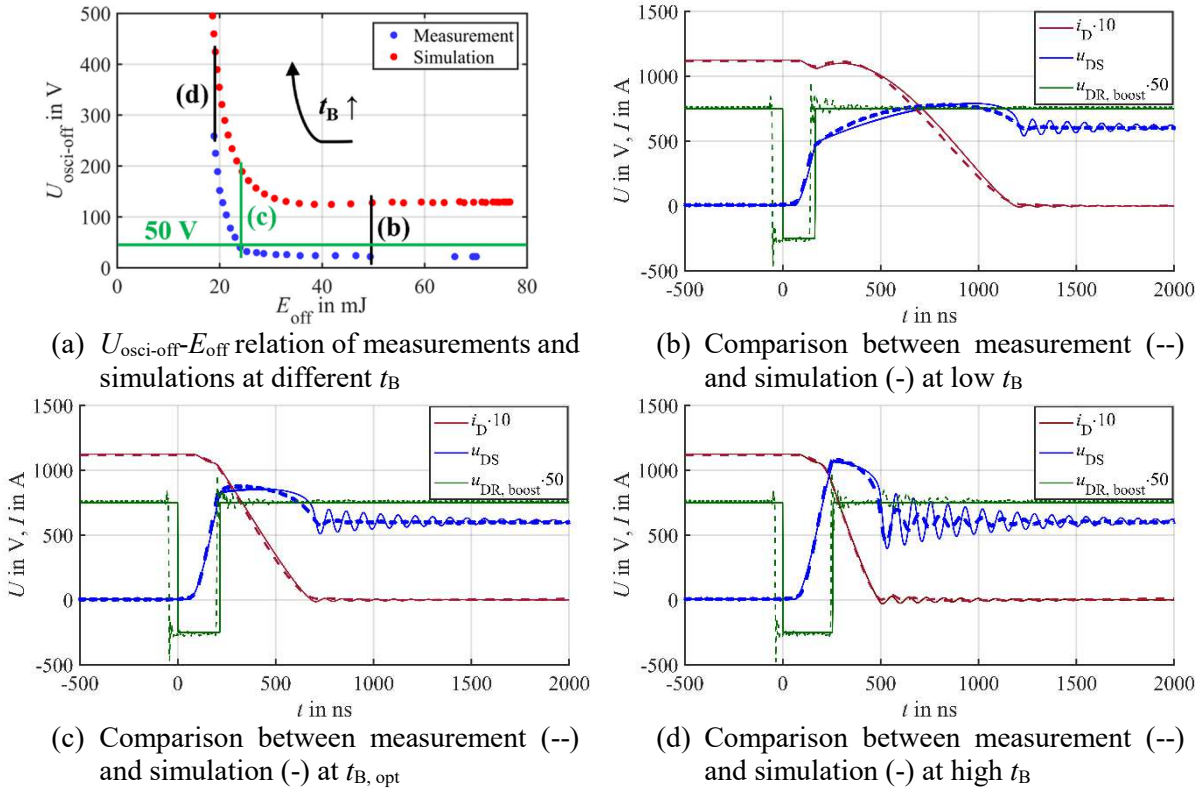

(a) $U_{osci-off}$-E_{off} relation of measurements and simulations at different t_B

(b) Comparison between measurement (--) and simulation (-) at low t_B

(c) Comparison between measurement (--) and simulation (-) at $t_{B, opt}$

(d) Comparison between measurement (--) and simulation (-) at high t_B

Fig. 3: Comparison between measurements and simulations of the boost-method implemented at SiC MOSFET turn-off at the test condition: U_{DC} = 600 V, I_D = 112 A, T_j = 25°C

Table II: Comparison between measurements and simulations shown in Fig. 3 (b) – (d)

	Measurements shown in dashed lines			Simulations shown in solid lines		
Figure	t_B/ns	$U_{osci-off}$/V	E_{off}/mJ	t_B/ns	$U_{osci-off}$/V	E_{off}/mJ
Fig. 3 (b)	195	22	49.4	165	128	49.8
Fig. 3 (c)	245	40	24.0	215	189	24.4
Fig. 3 (d)	285	259	18.9	255	424	19.2

To investigate the influence of the boost-time t_B on the switching performance, a test series of boost-switching processes are performed with different t_B under the test condition: U_{DC} = 600 V, I_D = 112 A, T_j = 25°C. The voltage oscillation indicator at SiC MOSFET turn-off $U_{osci-off}$ is quantitively defined as $|U_1 - U_2|$, as shown in Fig. 2 (b). The relation between $U_{osci-off}$ and the turn-off switching losses E_{off} in respect to t_B is shown in Fig. 3 (a) as discrete blue points. Each blue point represents a boost-switching

measurement with a certain t_B. It can be seen that with increasing t_B, E_{off} decreases and $U_{osci\text{-}off}$ increases monotonously. A trade-off exists between $U_{osci\text{-}off}$ and E_{off}. The maximum t_B with an $U_{osci\text{-}off}$ of no more than a predefined threshold of the oscillation amplitude is defined as the optimum boost-time $t_{B,\,opt}$. When the threshold value is set as $U_{osci\text{-}off}$ = 50 V, the boost-switching process with $t_{B,\,opt}$ is represented by the crossing point of the two green lines shown in Fig. 3 (a). The corresponding switching process is shown in dashed lines in Fig. 3 (c). The switching characteristics of the three measurements shown in dashed lines in Fig. 3 (b), Fig. 3 (c) and Fig. 3 (d) are listed in Table II left. $t_B < t_{B,\,opt}$ leads to high losses, as the switching process shown in dashed lines in Fig. 3 (b), while $t_B > t_{B,\,opt}$ leads to high oscillation amplitudes, as the switching process shown in dashed lines in Fig. 3 (d). Thus, t_B must be set as optimum. As the di/dt-signal is proportional to the voltage oscillation during switching transients, $U_{osci\text{-}off}$ can be determined by the voltage drop from the power source to the kelvin source for reduced measuring effort.

A simulation series of boost-switching processes is performed with different t_B at the same condition as the test series. The relation between the voltage oscillation indicator at SiC MOSFET turn-off $U_{osci\text{-}off}$ and the turn-off switching losses E_{off} is shown in Fig. 3 (a) as red points. Each red point represents a boost-switching simulation with a certain t_B. It can be seen that the $U_{osci\text{-}off}$-E_{off} relation of the test series and the $U_{osci\text{-}off}$-E_{off} relation of the simulation series are qualitatively identical with an oscillation offset. Three boost-switching simulations with different t_B are shown in solid lines in Fig. 3 (b), Fig. 3 (c) and Fig. 3 (d), respectively. The simulated boost-switching trajectories match well with the measured boost-switching trajectories. The switching characteristics of the three simulations are listed in Table II right. E_{off} of the compared measurements and simulations in Fig. 3 (b) – Fig. 3 (d) are almost equal, whereas t_B and $U_{osci\text{-}off}$ of the compared measurements and simulations are shifted by an offset. It is proven that the proposed simulation model can be used to qualitatively investigate the boost-switching performance.

3.2 Optimization of turn-on switching performance

The variant of the boost-method for the optimization of SiC MOSFET turn-on switching performance takes the advantages of the parasitic turn-on (PTO) effect to combine low switching losses and low EMI. The working principle of this variant is shown in Fig. 4 [7]. In case $I_D > 0$, the high side switch (HSS) performs a hard switching process and is called active switch (blue). The low side switch (LSS) acts as freewheeling device and is referred to as passive switch (red). The low boost gate resistance $R_{G,\,boost\text{-}off}$ accelerates the gate discharging, while the high gate resistance $R_{G,\,normal}$ decelerates it. The active turn-on of HSS is controlled by the turn-on gate resistance $R_{G,\,on}$, which is set to a low value for low switching losses. The control signals, the output voltages of the normal-drivers $U_{DR,\,normal}$ and the boost-drivers $U_{DR,\,boost}$ are shown in Fig. 4 right. Different from the variant of the boost-method implemented at SiC MOSFET turn-off (active turn-off), this variant is implemented at diode turn-off (passive turn-off). In order to avoid short circuit of the phase, a dead time t_D is set between the passive turn-off of LSS and the active turn-on of HSS. In other aspects, the two variants of the boost-method are similar.

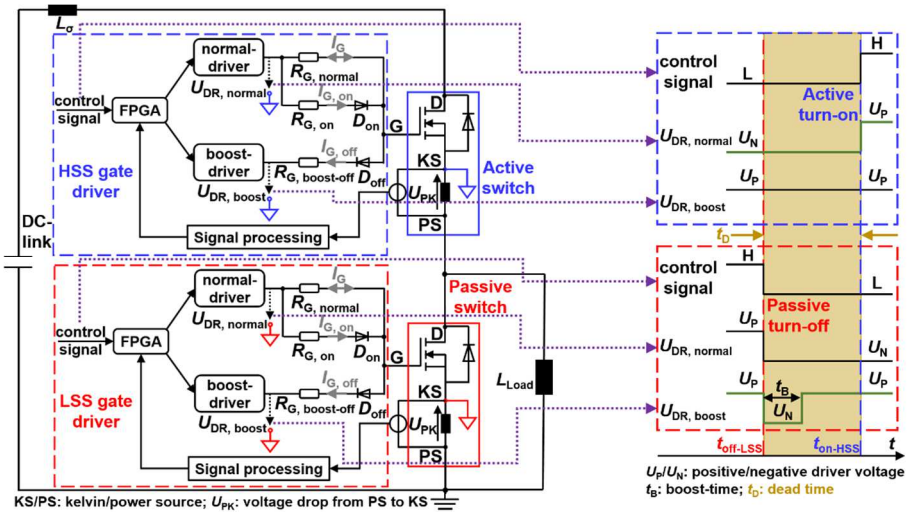

Fig. 4: Working principle of the boost-method for the optimization of SiC MOSFET turn-on switching performance with the control signals and output voltages of HSS/LSS gate drivers [7]

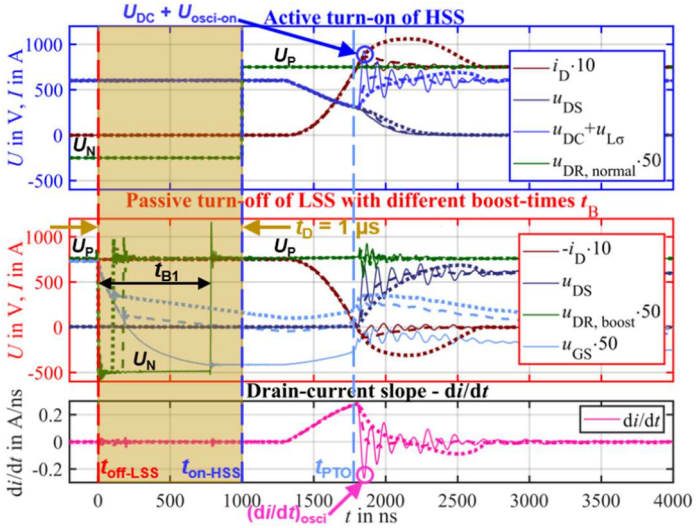

Test Nr.	1	2	3
Mark	Solid (-)	Dashed (--)	Dotted (⋯)
t_B/ns	780	170	100
$U_{osci-on}$/V	330	42	90
E_{MOS}/mJ	8.4	9.1	11.7
E_{Dio}/mJ	0.5	1.1	9.0
E_{on}/mJ	8.9	10.2	20.7
$E_{on} = E_{MOS} + E_{Dio}$			

Fig. 5: Comparison between boost-method controlled switching processes with different t_B at the test condition: t_D = 1 µs, I_D = 75 A, U_{DC} = 600 V, T_j = 25°C [7]

The switching trajectories of three boost-method controlled measurements with different boost-time t_B is illustrated in Fig. 5 left. The HSS signals are shown in the top diagram, the LSS signals in the middle diagram and the drain-current slope di/dt in the bottom diagram. With reducing t_B the three switching processes are shown in solid, dashed and dotted lines, respectively. In the middle diagram of Fig. 5 left it can be seen that the adaption of the gate source voltage u_{GS} affected via t_B results in the same control effect as the adjustment of the negative driver voltage U_N. Lower t_B leads to higher u_{GS} at the start time of the PTO effect t_{PTO}, which results in stronger PTO. A high overvoltage at the LSS will induce an oscillation between the commutation circuit stray inductance L_σ and the LSS junction capacitance. The occurrence of the PTO dampens the overvoltage and reduces the switching oscillation. The switching characteristics of the three switching processes are demonstrated in Fig. 5 right. The voltage oscillation indicator at SiC MOSFET turn-on $U_{osci-on}$ is quantitively defined as the maximum voltage oscillation peak of L_σ, as shown in the top diagram of Fig. 5 left. The total switching losses at SiC MOSFET turn-on E_{on} is defined as the cumulated switching losses of the active MOSFET E_{MOS} and the passive body-diode E_{Dio}. The switching process shown in solid lines has a high $U_{osci-on}$ of 330 V due to insufficient PTO. The switching process shown in dotted lines has a low $U_{osci-on}$ of 90 V, but the shoot-through current caused by PTO is high, which leads to high E_{Dio} of 9 mJ. The switching process shown in dashed lines achieves low $U_{osci-on}$ of 42 V and low E_{Dio} of 1.1 mJ simultaneously.

To investigate the influence of the boost-time t_B on the switching performance, a test series of boost-switching processes are performed with different t_B at the test condition: I_D = 75 A, U_{DC} = 600 V, T_j = 25°C, t_D = 1 µs. The relation between the voltage oscillation indicator at SiC MOSFET turn-on $U_{osci-on}$ and the total switching losses at SiC MOSFET turn-on E_{on} in respect to t_B is illustrated in Fig. 6 (a) as discrete blue points. Each blue point represents a boost-switching measurement with a certain t_B. It can be seen that with decreasing t_B, $U_{osci-on}$ first decreases significantly with negligible increase of losses. Almost no losses are generated in the passive switch until $U_{osci-on}$ reaches its minimum. However, with further decreasing t_B, E_{on} rises dramatically due to excessive PTO. $U_{osci-on}$ increases not because of increasing oscillation, but caused by the increasing PTO current. The switching event shown in dotted lines in Fig. 5 left demonstrates this phenomenon. High t_B leads to high oscillation, while low t_B to high losses. Hence, t_B must be set appropriate. As E_{on} decreases with increasing t_B monotonously, the maximum t_B with an $U_{osci-on}$ of no more than a predefined oscillation threshold is defined as optimum boost-time $t_{B,\,opt}$. If the oscillation threshold is set as $U_{osci-on}$ = 50 V, the boost-switching process with $t_{B,\,opt}$ is marked with the green circle shown in Fig. 6 (a), which is corresponded to the switching process shown in dashed lines in Fig. 5 left and Fig. 3 (c).

A simulation series of boost-switching processes is performed with different t_B at the same test condition as the test series. The relation between $U_{osci-on}$ and E_{on} is shown in Fig. 6 (a) as red points. Each red point

represents a boost-switching simulation with a certain t_B. It can be seen that the $U_{osci\text{-}on}$-E_{on} relation of the measurement series matches well with the $U_{osci\text{-}on}$-E_{on} relation of the simulation series with a slight difference of E_{on}. Three comparisons of switching trajectory between measurement and simulation with different t_B are shown in Fig. 6 (b), Fig. 6 (c) and Fig. 6 (d), respectively. Their switching characteristics are listed in Table III. The switching trajectories, the PTO effect and the influence of t_B on the boost-switching performance are well simulated by the proposed model.

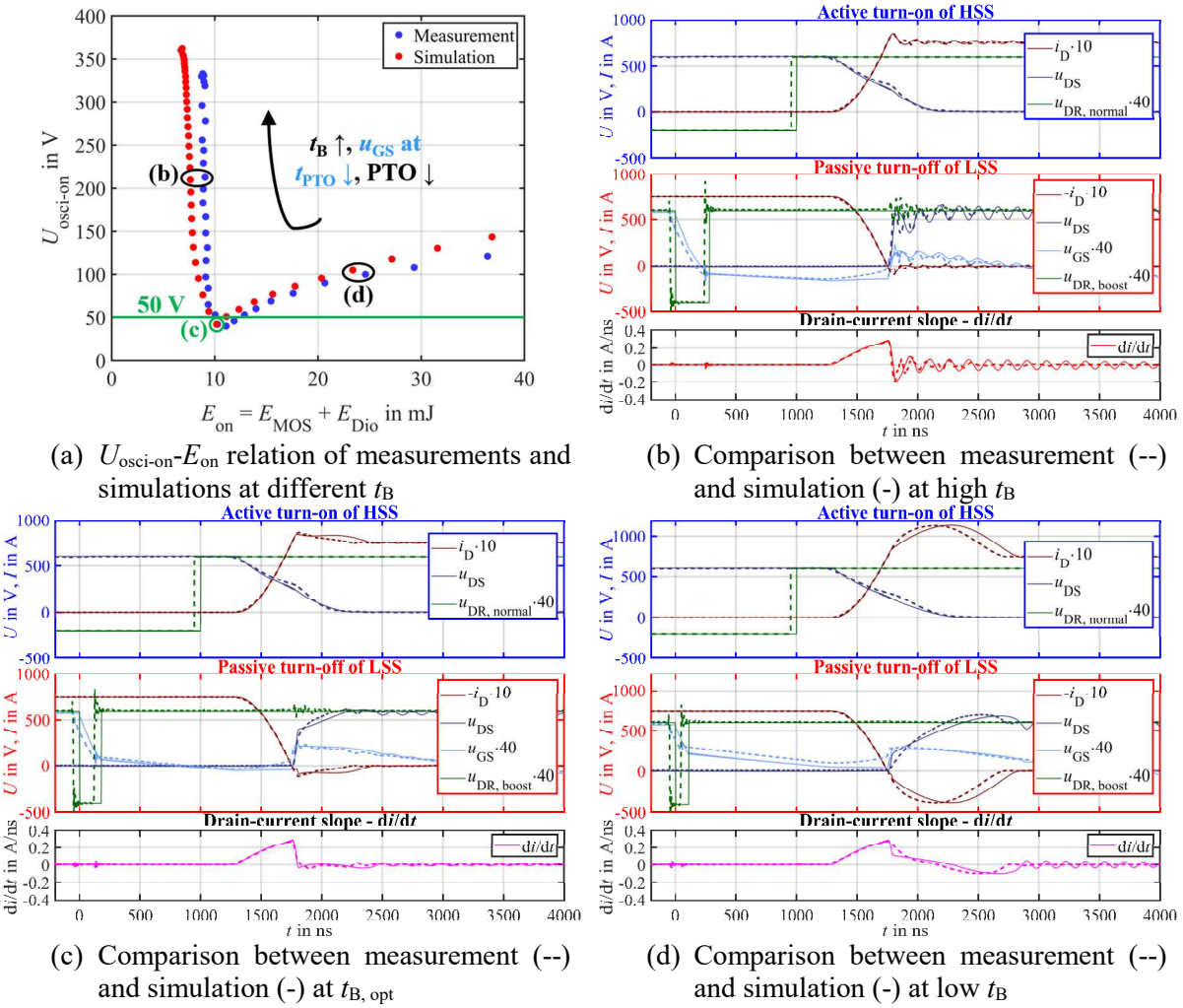

(a) $U_{osci\text{-}on}$-E_{on} relation of measurements and simulations at different t_B

(b) Comparison between measurement (--) and simulation (-) at high t_B

(c) Comparison between measurement (--) and simulation (-) at $t_{B,\,opt}$

(d) Comparison between measurement (--) and simulation (-) at low t_B

Fig. 6: Comparison between measurements and simulations of the boost-method implemented at diode turn-off at the test condition: t_D = 1 µs, I_D = 75 A, U_{DC} = 600 V, T_j = 25°C

Table III: Comparison between measurements and simulations shown in Fig. 6 (b) – (d)

	Measurements shown in dashed lines			Simulations shown in solid lines		
Figure	t_B/ns	$U_{osci\text{-}on}$/V	E_{on}/mJ	t_B/ns	$U_{osci\text{-}on}$/V	E_{on}/mJ
Fig. 6 (b)	280	213	9.1	280	210	7.6
Fig. 6 (c)	170	42	10.2	180	42	10.2
Fig. 6 (d)	90	100	24.6	110	105	23.4

4 Optimization of switching performance in continuous operation

In this section, only the tracking method implemented at SiC MOSFET turn-off is discussed. Simulation and measurement of PWM controlled continuous operation are performed with the proposed gate control approach at the same condition. Their switching characteristics are compared. The performance of the proposed approach is compared with the performance of a simple gate control with a single gate resistor.

4.1 Review of the tracking method at SiC MOSFET turn-off

It is verified by measurements that the optimum boost-time $t_{B,\,opt}$ is strongly dependent on the operating condition, compare [6]. To realize an operating condition dependent gate control, the tracking method is developed. Its working principle is shown in Fig. 7. The basic idea of the tracking method is to trace varying $t_{B,\,opt}$ through the iteration of t_B according to the result of oscillation evaluation. During every boost-switching process, the di/dt-signal is measured and processed for oscillation evaluation. A switching process with an oscillation of no more than the predefined oscillation threshold is considered as oscillation-free. Therefore, $t_{B,\,opt}$ is the maximum t_B for an oscillation-free switching process. The tracking method control loop is closed over the next switching process. The boost-time of the actual switching process $t_{B,\,act}$ is not adjusted for the actual switching process, but the next one. As shown in Fig. 3 (a), the voltage oscillation indicator $U_{osci\text{-}off}$ increases monotonously with increasing t_B. If an oscillation is detected in the actual switching process, it means that $t_{B,\,act} > t_{B,\,opt}$. $t_{B,\,act}$ will be decremented with Δt_B for the next switching process. Otherwise, $t_{B,\,act} <= t_{B,\,opt}$. $t_{B,\,act}$ will be incremented with Δt_B for the next switching process. $t_{B,\,act}$ is assumed to be maintained within a narrow band around the varying $t_{B,\,opt}$ by the tracking method. A more detailed explanation of the tracking method is presented in [6].

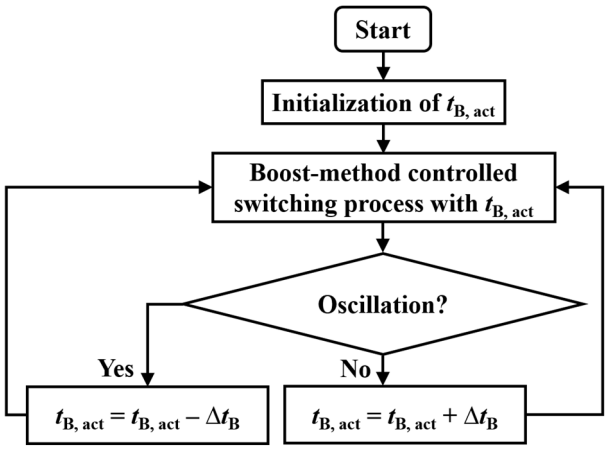

Fig. 7: Working principle of the tracking method

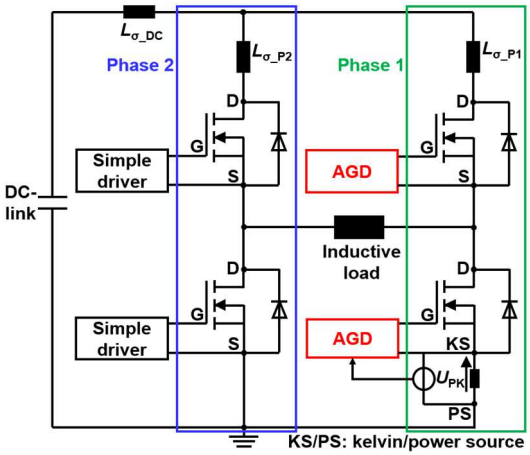

Fig. 8: Circuit diagram of the test setup

4.2 Implementation of the tracking method in continuous operation

The equivalent circuit diagram of the H-Bridge measurement setup is shown in Fig. 8. The AGDs (red) are connected to phase 1 (green). A test of PWM controlled continuous operation with a fundamental frequency $f_f = 60$ Hz, a switching frequency $f_{sw} = 10$ kHz, a dead time $t_D = 3$ µs and a finite number of periods $N_P = 5$ is performed under the test condition: $U_{DC} = 550$ V, $T_j = 25$°C. The drain-current course $I_D(t)$ is sinusoidal. The increment of the actual boost-time $t_{B,\,act}$ is set as $\Delta t_B = 5$ ns. In the performance evaluation, every turn-off switching process is extracted from the continuous operation and separately evaluated. Different switching characteristics of each turn-off switching process with $I_D > 0$ are evaluated and plotted as discrete points in different diagrams of Fig. 9 (a). For turn-off switching processes with $I_D < 0$, the actual boost-time $t_{B,\,act}$ is evaluated, the voltage oscillation indicator $U_{osci\text{-}off}$ and the turn-off switching losses E_{off} are always set as 0. U_{DC} and I_D are shown in the top diagram, $t_{B,\,act}$ in the second diagram, $U_{osci\text{-}off}$ in the third diagram and E_{off} in the bottom diagram. $t_{B,\,act}$, $U_{osci\text{-}off}$ and E_{off} of the measurement are shown in black. As the energy stored in the DC-link capacitors is consumed during continuous operation because of a power limitation of the DC voltage source, U_{DC} and the amplitude of sinusoidal I_D decrease with time as shown in the top diagram. It can be seen that $t_{B,\,act}$ increases monotonously at the start-up as $U_{osci\text{-}off}$ is much lower than the oscillation threshold. After the threshold is reached, $U_{osci\text{-}off}$ is maintained in close proximity to the threshold, as varying $t_{B,\,opt}$ caused by varying I_D, U_{DC} is traced by $t_{B,\,act}$ with an apparent concave trajectory. The behavior of the tracking method in the driving cycle meets the expectations.

A simulation of continuous operation is performed. The I_D- and U_{DC}-course of the measurement shown in the top diagram of Fig. 9 (a) are utilized as simulation condition to ensure a fair comparison. The

switching characteristics of every simulated turn-off switching process are evaluated and plotted as discrete green points in Fig. 9 (a) in the same manner as the measurement. It can be seen that the E_{off}-courses of the simulation and the measurement are almost equal, whereas the $t_{B,act}$- and $U_{osci-off}$-courses of the simulation and the measurement show an offset, which is consistent with the comparisons of single operating point between simulations and measurements shown at the end of section 3.1. Fig. 9 (b) illustrates a comparison of the switching trajectories at t = 24.62 ms between the simulation shown in solid lines and the measurement shown in dashed lines. The simulated boost-switching trajectory matches well with the measured boost-switching trajectory. It is proven that the proposed SiC MOSFET behavior simulation model is capable of qualitatively investigating the proposed gate control approach consisting of the boost-method and the tracking method, even in continuous operation.

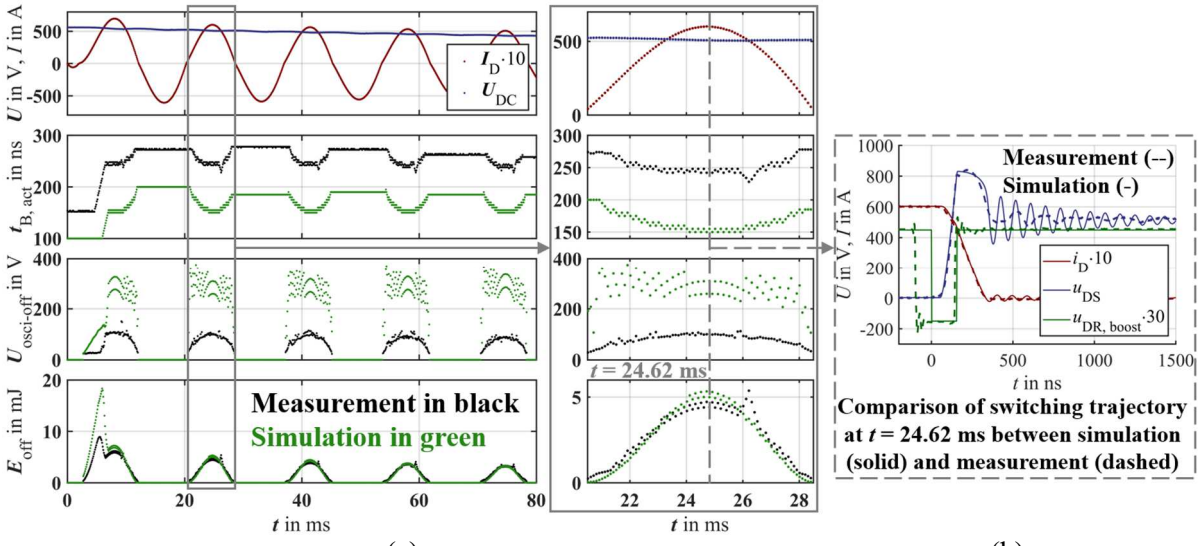

(a) (b)

Fig. 9: Performance comparison of PWM controlled continuous operation between measurement (black points in Fig. 9 (a), dashed lines in Fig. 9 (b)) and simulation (green points in Fig. 9 (a), solid lines in Fig. 9 (b)) at the condition: f_f = 60 Hz, f_{sw} = 10 kHz, U_{DC} = 550 V, T_j = 25°C, sinusoidal I_D

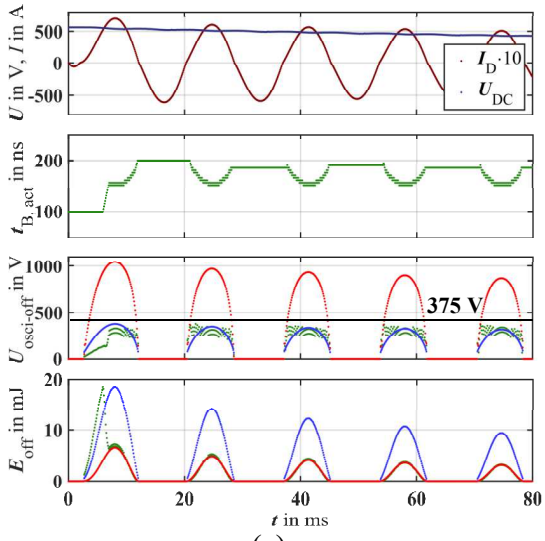

Gate control Type	Mark	$U_{osci-off-max}$ in V	$E_{off-total}$ in J
Proposed gate control	**Green**	**375 (36%)**	**0.69 (30%)**
Simple gate control with slow speed	Blue	375 (36%)	2.27 (100%)
Simple gate control with fast speed	Red	1043 (100%)	0.70 (31%)

(a) (b)

Fig. 10: Performance comparison of continuous operation between simulations of the proposed gate control (green) and simple gate control (fast in red, slow in blue) at the condition shown in Fig. 9

$$E_{off-total} = \sum_{n=1}^{N_S} E_{off-n}, N_S = \frac{f_{sw}}{f_f} \cdot N_P \quad (1)$$

To investigate the performance of the proposed gate control approach, two simulations of continuous operation are performed with different switching speeds at the same condition as the simulation shown in Fig. 9. Their gate control type is simple gate control with a single gate resistance. Fig. 10 demonstrates a performance comparison between these two simulations with simple gate control and the simulation with the proposed approach shown in Fig. 9. The switching characteristics of every simulated turn-off switching process are evaluated and plotted as discrete points in Fig. 10 (a) in the same way as Fig. 9 (a). The proposed approach is shown in green, the slow simple gate control in blue and the fast in red. The maximum voltage oscillation indicator of continuous operation $U_{\text{osci-off-max}}$ is defined to evaluate the oscillation magnitude. The total turn-off switching losses of continuous operation $E_{\text{off-total}}$ is calculated by means of Eq. (1). N_{S} is the total number of turn-off switching events of continuous operation, N_{P} the number of periods and $E_{\text{off-n}}$ the losses of the "n"-th turn-off switching process. It should be pointed out that the calculation of $E_{\text{off-total}}$ starts from the second period, as the transition of $t_{\text{B, act}}$ from start-up to $t_{\text{B, opt}}$ leads to an E_{off}-peak, as shown in the bottom diagram of Fig. 9 (a), Fig. 10 (a). It can be concluded from the table shown in Fig. 10 (b) that $E_{\text{off-total}}$ of the proposed gate control is 70% lower than $E_{\text{off-total}}$ of the slow simple gate control while $U_{\text{osci-off-max}}$ is equal for the two control techniques. $U_{\text{osci-off-max}}$ of the proposed gate control is 64% lower than that of the fast simple gate control without increased $E_{\text{off-total}}$. The performance of the proposed gate control in continuous operation is proven to be excellent.

5 Conclusion

A SiC MOSFET behavior model is proposed to simulate a boost-method for the switching performance optimization of a single operating point and a tracking method for the dynamic optimization of varying operating conditions. The simulated boost-switching trajectories are consistent with the measured ones of a SiC MOSFET at both turn-off and turn-on. The tracking method is investigated by simulations and measurements of PWM controlled continuous operation. The simulated behavior of the tracking method matches well with the measured behavior. The tracking method is capable of dynamically optimizing switching performance for varying operating conditions. It is proven by simulation that the performance of the proposed gate control approach consisting of the boost-method and the tracking method is significantly better than the performance of simple gate control in continuous operation. 70% of the switching losses or 64% of the oscillation amplitude can be reduced without increased oscillation amplitude or switching losses, respectively.

6 References

[1] E. U. Krafft, B. Laska, A. Nagel and J. Weigel: A new standard IGBT housing for high-power converters, EPE'15 ECCE Europe, pp. 1-11, 2015.

[2] A. Paredes, H. Ghorbani, V. Sala, E. Fernandez and L. Romeral: A new active gate driver for improving the switching performance of SiC MOSFET, 2017 IEEE APEC, pp. 3557-3563, 2017.

[3] M. R. Ahmed, R. Todd and A. J. Forsyth: Predicting SiC MOSFET behavior under hard-switching, soft-switching, and false turn-on conditions, IEEE Transactions on Industrial Electronics, vol. 64, no. 11, pp. 9001-9011, 2017.

[4] Z. Miao, Y. Mao, C.-M. Wang and K. D. T. Ngo: Detection of cross-turn-on and selection of off drive voltage for an SiC power module, IEEE Transactions on Industrial Electronics, vol. 64, no. 11, pp. 9064-9071, 2017.

[5] S. Zhao, X. Zhao, Y. Wei, Y. Zhao and H. A. Mantooth: A review of switching slew rate control for silicon carbide devices using active gate drivers, IEEE Journal of Emerging and Selected Topics in Power Electronics, vol. 9, no. 4, pp. 4096-4114, 2021.

[6] Z. Li, R. W. Maier, Mark-M. Bakran, D. Domes and F.-J. Niedernostheide: How to turn off SiC MOSFET with low losses and low EMI across the full operating range, PCIM Europe 2021, pp. 1263-1270, 2021.

[7] Z. Li, R. W. Maier, M. Walter and Mark-M. Bakran: A self-regulating gate control based on the parasitic turn-on effect for low losses and low EMI of SiC MOSFET, PCIM Europe 2022, 2022.

[8] R. W. Maier and Mark-M. Bakran: Switching SiC MOSFETs under conditions of a high power module, EPE'18 ECCE Europe, pp. 1-10, 2018.

[9] P. Hofstetter, R. W. Maier and Mark-M. Bakran: Influence of the threshold voltage hysteresis and the drain induced barrier lowering on the dynamic transfer characteristic of SiC power MOSFETs, 2019 IEEE APEC, pp. 944-950, 2019.

[10] P. Hofstetter and Mark-M. Bakran: Mitigating drain source voltage oscillation for SiC power MOSFETs in order to reduce electromagnetic interference, EPE'19 ECCE Europe, pp. 1-10, 2019.